minerals

MDPI

Article

A Petrologic and Noble Gas Isotopic Study of New Basaltic Eucrite Grove Mountains 13001 from Antarctica

Chuantong Zhang [1,2,3,4], Bingkui Miao [1,3,*], Huaiyu He [5], Hongyi Chen [1,3], P. M. Ranjith [5] and Qinglin Xie [4]

1 Institution of Meteorites and Planetary Materials Research, Guilin University of Technology, Guilin 541006, China; zct@glut.edu.cn (C.Z.); chy@glut.edu.cn (H.C.)
2 Key Laboratory of Lunar and Deep Space Exploration, Chinese Academy of Sciences, Beijing 100029, China
3 Guangxi Key Laboratory of Hidden Metallic Ore Deposits Exploration, Guilin University of Technology, Guilin 541006, China
4 College of Environmental Science and Engineering, Guilin University of Technology, Guilin 541006, China; xql@glut.edu.cn
5 Key Laboratory of Earth and Planetary Physics, Institute of Geology and Geophysics, Chinese Academy of Sciences, Beijing 100029, China; huaiyuhe@mail.iggcas.ac.cn (H.H.); ranjith@mail.iggcas.ac.cn (P.M.R.)
* Correspondence: miaobk@glut.edu.cn

Abstract: Howardite-Eucrite-Diogenite (HED) meteorite clan is a potential group of planetary materials which provides significant clues to understand the formation and evolution of the solar system. Grove Mountains (GRV) 13001 is a new member of HED meteorite, recovered from the Grove Mountains of Antarctica by the Chinese National Antarctic Research Expedition. This research work presents a comprehensive study of the petrology and mineralogy, chemical composition, noble gas isotopes, cosmic-ray exposure (CRE) age and nominal gas retention age for the meteorite GRV 13001. The output data indicate that GRV 13001 is a monomict basaltic eucrite with typical ophitic/subophitic texture, and it consists mainly of low-Ca pyroxene and plagioclase with normal eucritic chemical compositions. The noble gas based CRE age of the GRV 13001 is approximately 29.9 ± 3.0 Ma, which deviates from the major impact events or periods on the HED parent body. Additionally, the U,Th-^{4}He and ^{40}K-^{40}Ar gas retention ages of this meteorite are ~2.5 to 4.0 Ga and ~3.6 to 4.1 Ga, respectively. Based on the noble gases isotopes and the corresponding ages, GRV 13001 may have experienced intense impact processes during brecciation, and weak thermal event after the ejection event at approximately 30 Ma.

Keywords: Antarctic eucrite GRV 13001; petrology and mineralogy; noble gas; CRE age; gas retention age

check for updates

Citation: Zhang, C.; Miao, B.; He, H.; Chen, H.; Ranjith, P.M.; Xie, Q. A Petrologic and Noble Gas Isotopic Study of New Basaltic Eucrite Grove Mountains 13001 from Antarctica. *Minerals* **2021**, *11*, 279. https://doi.org/10.3390/min11030279

Academic Editor: Roman Skála

Received: 3 February 2021
Accepted: 6 March 2021
Published: 9 March 2021

Publisher's Note: MDPI stays neutral with regard to jurisdictional claims in published maps and institutional affiliations.

Copyright: © 2021 by the authors. Licensee MDPI, Basel, Switzerland. This article is an open access article distributed under the terms and conditions of the Creative Commons Attribution (CC BY) license (https://creativecommons.org/licenses/by/4.0/).

1. Introduction

The Howardite-Eucrite-Diogenite (HED) clan is composed of the individual eucrite, diogenite, and howardite meteorite groups. Among the HEDs, the eucrites and diogenites are igneous rocks formed at different depths in their parent body, whereas the howardites are impact mixtures of these two [1,2]. Eucrites have surface reflectance spectra similar to those of the asteroid 4 Vesta, which thus helped McCord et al. (1970) [3] to propose that the HEDs may have originated from Vesta. The subsequent discovery of V-type asteroids near the gravitational resonance region of the asteroid belt [4] implies a possible transfer mechanism of the HED meteorites from Vesta to Earth [5] from the dynamics perspective. Therefore, there has been a wide consensus that the HEDs may come from Vesta or V-type asteroids ejected from Vesta [1,2], although this has been challenged by the discovery of anomalous oxygen isotopes in few eucrites recently [6–9]. Except for lunar and Martian meteorites, the HEDs are the only available group of meteorites which may have a genetic link with definite parent asteroid [10]. As the second largest existing asteroid in the asteroid belt, Vesta is an important research object to understand and explore the early differentiation and evolutionary history of the Solar System [1,2,11]. Meanwhile, the HEDs

are currently the largest collection of stony differentiated meteorites [10]; hence, they help to address diverse scientific issues associated the aforementioned research. Thus, HEDs and their parent body are potential planetary material/body that provides significant clues to understand the formation and evolution of the solar system.

Noble gases are an important group of elements that can help to elucidate the impact and thermal history of the HED meteorites and their parent body (e.g., [12,13]). After the meteorite launched from its parent body and transited to Earth, cosmogenic noble gases have been produced by exposure to high-energy cosmic-ray particles. The time over which a meteorite is exposed to cosmic rays can be obtained based on noble gases, i.e., cosmic-ray exposure (CRE) age, which indicates the time at which the meteoroid was ejected from its parent body [14–17]. According to the CRE age distribution, general consensus is that more than one-third of all HEDs were ejected from the parent body by two major impact events that occurred at ~20 Ma and ~40 Ma, respectively [13,15,17]. Additionally, there are at least 5–10 other impact events to account for the CRE ages of the remaining HEDs [12,18], indicating these meteorites were ejected from parent body by impact events other than those at ~20 Ma and ~40 Ma. On the other hand, the radiogenic noble gases ^{4}He (U,Th decay) and ^{40}Ar (^{40}K decay) began to accumulate in the meteoritic matter after it cooling below the closure temperature of these radiogenic noble gases [19–21]. The corresponding radioactive decay ages are called as gas retention ages of U,Th-^{4}He (T_4) and ^{40}K-^{40}Ar (T_{40}). Ideally, these gas retention ages characterize the crystallization time of meteoritic matter. Whereas, subsequent impact and thermal events can reset these isotopic systems, thus these ages provide thermal history information of the meteorite. Based on the K–Ar system, it is currently widely accepted that the HED meteorites and their parent body may have experienced degassing events caused by intense impacts or thermal events at ~3.45 to 3.55 Ga, ~3.8 Ga, ~3.9 to 4.0 Ga, and ~4.48 Ga [21,22].

The meteorite in focus of this study is GRV 13001 that was recovered from the Grove Mountains of Antarctica by the Chinese National Antarctic Research Expedition. This article presents a comprehensive study of the petrology and mineralogy, chemical composition, noble gas isotopes, cosmic-ray exposure age, and nominal gas retention age. Thus, details of classification of this meteorite, cosmic ray exposure and impact/thermal histories of the GRV 13001 are discussed in different sections below. In addition, this work also adds new valuable data support for understanding the collisional history of HED parent bodies.

2. Sample and Experiment

2.1. Sample Preparation

GRV 13001 was initially classified as a monomict eucrite from the Grove Mountain collected by the Chinese National Antarctic Research Expedition in 2014 [23,24]. Its weight and size were 1.3 kg and 8.5 × 9.6 × 9.0 cm^3, respectively, with a residual black fusion crust. A sample of ~2 × 2 cm^2 in size was cut for use in this study using various techniques. The preparation process was as follows (Figure 1): (1) A sample of ~210 mg, Clast1, was extracted at the left side of Section 1, from which a polished thin Section A was made (Figure 1a). (2) A sample of ~40 mg, Clast2, was collected at the bottom of Section 2, on which polished thin Section B was made (Figure 1b). (3) A sample of ~21 mg, Clast3, was isolated on the fracture surface (Figure 1c). (4) A sample with light-colored lithology (~100 mg) was selected as the Matrix sample, and then the fine-grained parts (~90 mg) of 3.5 g of meteorite fragments were collected as the Bulk sample. (5) The five samples were ground using an agate mortar for noble gas measurements (particle size > approximately 0.1–0.2 mm). Above clasts are relatively large and can be easily separated from the hand specimen of meteorite. Therefore, it can be ensured that the samples obtained are clasts and have sufficient sample mass used for experiment analysis.

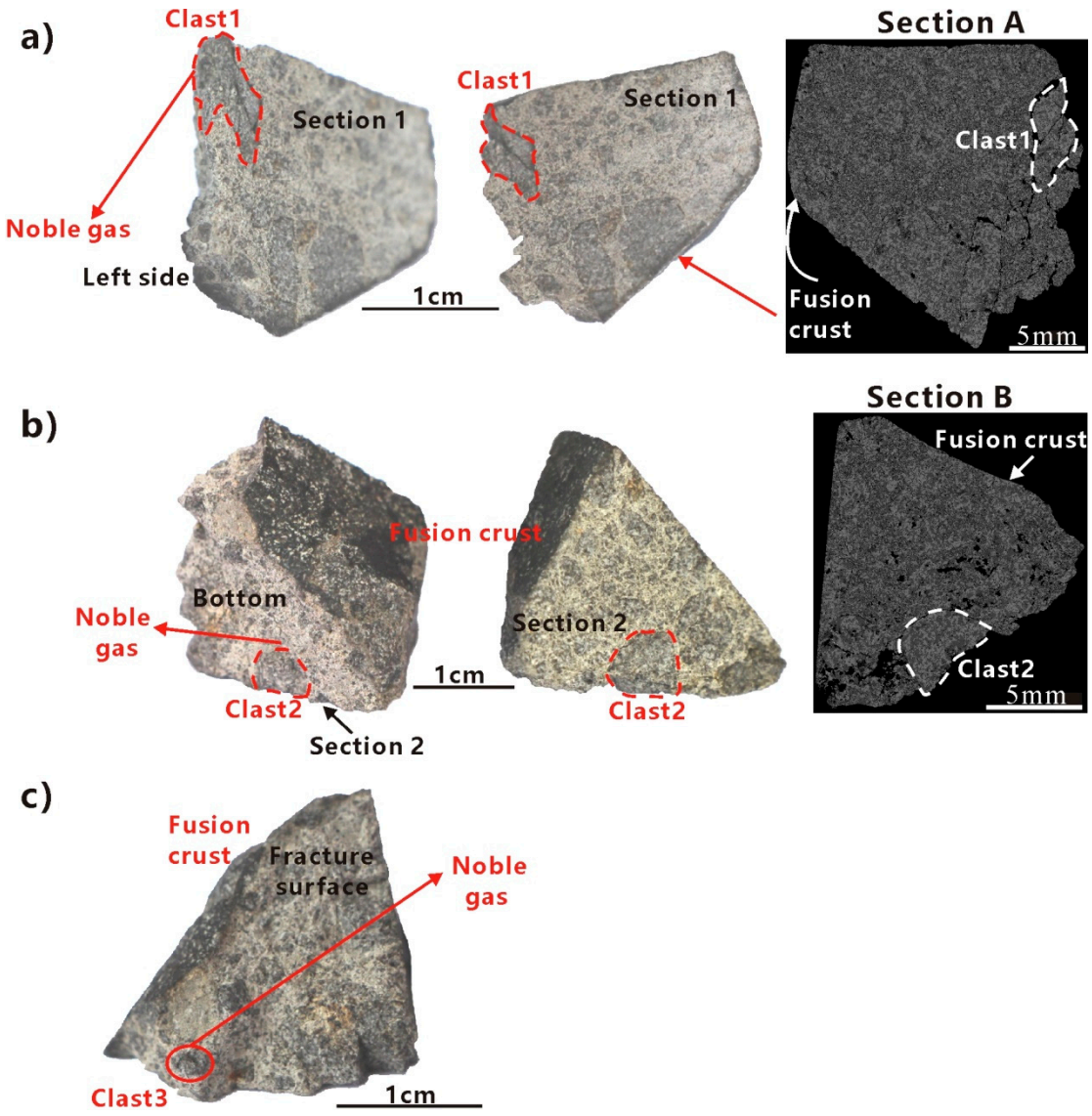


Figure 1. Schematic diagram of the sample preparation for the GRV 13001 meteorite. (**a**) Clast1, (**b**) Clast2, (**c**) Clast3. Two standard polished sections were made for lithology observation and chemical analysis; 3 clasts, 1 matrix and 1 bulk samples were prepared for noble gases measurement.

2.2. Lithology and Chemical Composition Analysis

The polished thin section preparation, petrographic observation and chemical composition analysis were performed at the Institution of Meteorites and Planetary Materials Research, Guilin University of Technology, Guilin, China. The structure, mineral association and extinction characteristics, and other optical properties of the meteorite were observed with a Nikon (NIKON ECLIPSE) 100POL advanced optical microscope (Nikon Corporation, Tokyo, Japan). JEOL JXA-8230 electron probe microanalysis (EPMA) (JEOL Ltd., Tokyo, Japan) was used to measure the chemical composition of the minerals and fusion crust. Chemical composition analyses were conducted with an accelerating potential of 15 keV, beam current of 20 nA, beam sizes of 1–10 μm, and 4 min count time. A combination of natural silicate and oxide minerals was utilized for calibration, and standard ZAF corrections were applied. The standard sample for the elements Si, Mg, and Fe is olivine, and their detection limits are 130 ppm, 119 ppm, and 154 ppm, respectively. The standard sample of Na and Al are albite, and their detection limits are 63 ppm and 47 ppm, respectively. The standard sample of Ca is wollastonite with a detection limit of

91 ppm. The standard sample of Cr is chromic oxide, and its detection limit is 259 ppm. The standard sample of Ti is rutile, and the detection limit is 294 ppm. Manganese oxide is the standard sample of Mn, whose detection limit is 104 ppm. The standard sample of V is calcium vanadate, and its detection limit is 281 ppm. Phlogopite is the standard sample of K, whose detection limit is 31 ppm. In addition, the mineral modal abundance of Section A and B were counted using the Adobe Photoshop software package.

2.3. Noble Gases Measurement

The abundance and isotopic ratios of noble gases were measured at the Institute of Geology and Geophysics, Chinese Academy of Sciences (Beijing, China), using a multi-collector Noblesse mass spectrometer from Nu Instruments. The technical details of Noblesse mass spectrometer and measurement procedures have been given in some of the previous studies [25–29]. Briefly, samples of Clast1 (3.76 mg), Clast2 (0.87 mg), Clast3 (0.94 mg), Matrix (2.33 mg), and Bulk (2.30 mg) were loaded into a laser sample chamber and preheated in vacuum at 120 °C for 3 days to remove absorbed atmospheric noble gases. A CO_2 laser was used to melt the samples in the continuous-wave mode with wavelength of 10.6 μm, beam size of 3 mm and power of ~13.5 W. All the samples were heated for ~20 min. The gases released from the samples were purified using a combination of cold trap (at liquid nitrogen temperature) and two sets of Zr-Al getters with one at room temperature (~25 °C) and another at higher temperature (~300 °C), to remove the active gases such as H_2O, CO_2, CO, N_2, H_2, CH_4, hydrocarbons, etc. Subsequently, He, Ne, and Ar were separated from each other based on the difference in the boiling point, i.e., Ar and Ne gases were adsorbed by the cold trap (at liquid nitrogen temperature) and cryopump (at 35 K) containing activated carbon, respectively. Finally, He, Ne and Ar were inlet into the mass spectrometer in sequence for the measurement. Each sample had released >99% of the total noble gas. System blank concentrations were < 0.1% for ^{3}He, <1% for ^{21}Ne, and <3% for ^{38}Ar.

During the mass spectrometric measurement, the ions with same charge-to-mass ratio will interfere with the measured noble gas isotopes, which need correction before estimating actual noble gas abundances and isotopic ratios. The resolution of Noblesse mass spectrometer (M/ΔM) is greater than 750, which is adequate to completely distinguish the peak position of $^{3}He^{+}$ and HD^{+}, but not enough to completely separate $^{40}Ar^{++}$ from $^{20}Ne^{+}$, and $^{44}CO_2{}^{++}$ from $^{22}Ne^{+}$. Therefore, estimating $^{20}Ne^{+}$ and $^{22}Ne^{+}$ amounts require an elemental interference correction. Meanwhile, the ion source region is provided with a cold trap, which greatly reduces the interference of $^{40}Ar^{++}$ to $^{20}Ne^{+}$; and the collector region is equipped with Zr-Al getter pump which helps to reduce decrease the interference of $^{44}CO_2{}^{++}$ to $^{22}Ne^{+}$. In addition, the cryopump (at 80 K) is kept in contact with the mass spectrometer region during neon measurement, to reduce the interference of H_2O^{+}, $^{40}Ar^{++}$, and $^{44}CO_2{}^{++}$ with the Ne isotopes. The sensitivities and instrumental mass discrimination coefficients of He, Ne, and Ar of the Noblesse were determined by standard air [30] and Helium Standard of Japan (HESJ) [31]. Finally, the concentrations and isotopic ratios of He, Ne, and Ar of GRV 13001 were obtained based on the sensitivities, mass discrimination coefficients, and sample signal values.

3. Results

3.1. Petrology and Chemical Compositions

GRV 13001 is a breccia with the clasts and mineral fragments of various sizes seen in a fine-grain matrix (Figures 1 and 2). The plagioclases in clasts occur as lath-shaped, euhedral crystals, and there are anhedral-subhedral pyroxenes distributed intergranularly, showing ophitic/subophitic texture (Figure 3). Meanwhile, the pyroxenes and feldspars of GRV 13001 are slightly broken and have normal extinction under the cross-polarized light. There are no shock-melted veins or obvious weathering alteration products seen in the polished thin sections. These characteristics indicate that the GRV 13001 meteorite is relatively unshocked and has undergone low level terrestrial alteration.

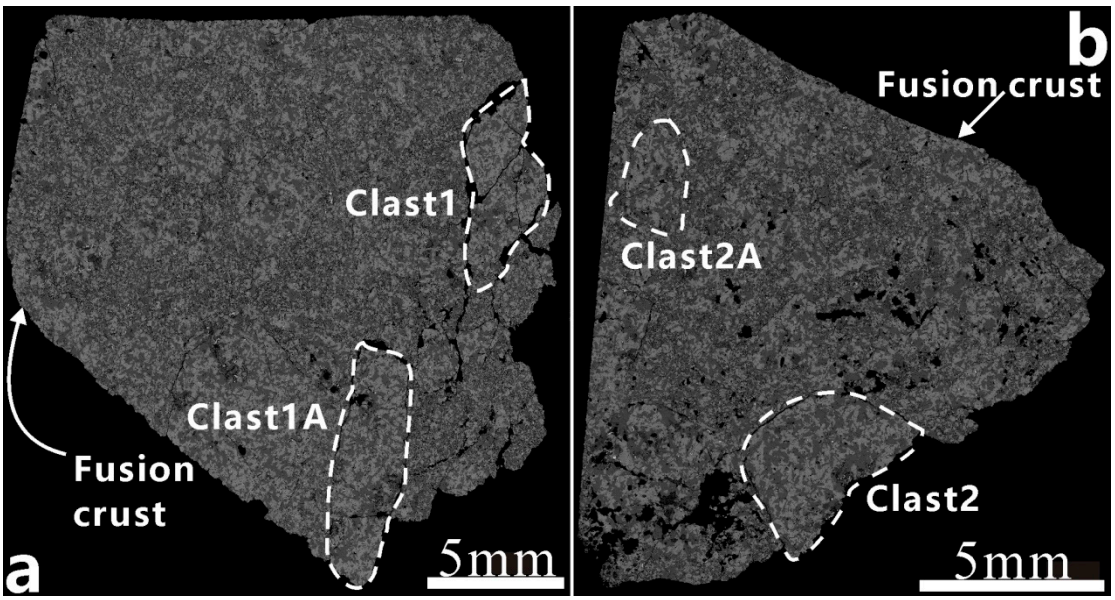


Figure 2. The backscattered electron (BSE) images of GRV 13001 showing a brecciated and ophitic/subophitic texture. (**a**) Section A, (**b**) Section B. The noble gas compositions of Clast1 and Clast2 have been measured in this work.

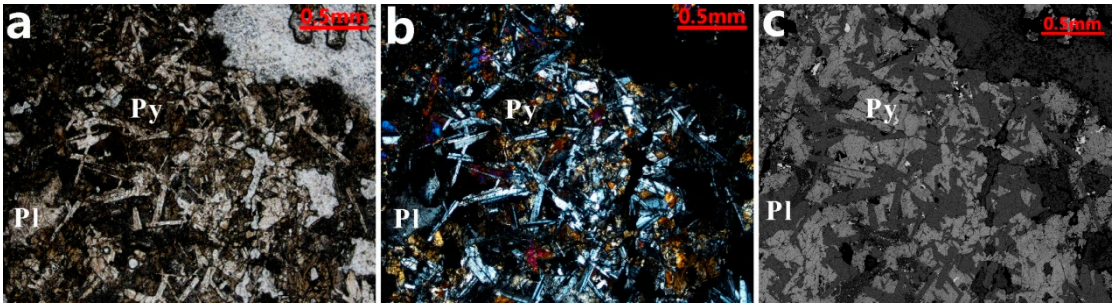


Figure 3. The ophitic-subophitic texture of the GRV 13001 meteorite. (**a**) plane-polarized light image; (**b**) cross-polarized light image; (**c**) backscattered electron image. The plagioclases (Pl) occur as lath-shaped, euhedral crystals, and there are anhedral-subhedral pyroxenes (Py) distributed intergranularly.

The clasts in GRV 13001 are mainly composed of pyroxene, plagioclase (~0.35 mm size) and a minor amount of silica phase, and a small amount of opaque minerals (such as Cr-spinel, ilmenite, and troilite) and zircons can also be observed. The matrix is composed of fine-grained minerals (<0.05 mm size), whose assemblage is consistent with the clasts. Although the majority of pyroxenes are low-Ca pyroxenes, high-Ca pyroxenes also exist as exsolution lamellaes in some areas. The sizes of zircons are less than 0.01 mm with two occurrences: one is associated with ilmenite and the other is irregularly shaped and does not coexist with ilmenite. In addition, the residual fusion crust enriched in spherical bubbles of different sizes can be found on the margin of sections (Figure 4). It appears light yellowish under plane-polarized light and black under cross-polarized light. The mineral modal abundances of two sections of GRV 13001 are similar (Figure 5), and the average value is as follows: pyroxenes (~45.6 vol.%), plagioclase (~46.8 vol.%), silica (~7.2 vol.%), and opaque minerals (~0.4 vol.%).

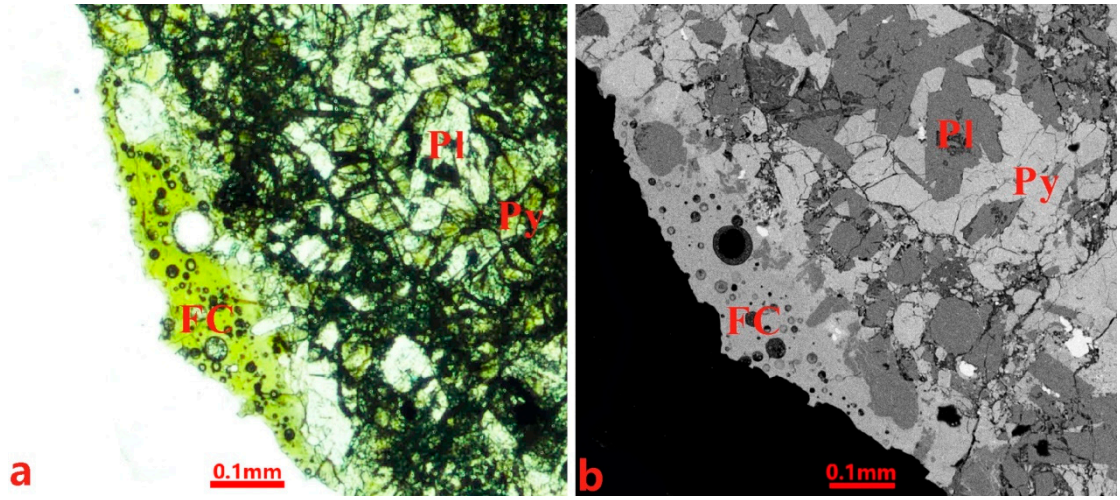


Figure 4. The fusion crust of the GRV 13001 meteorite. (**a**) plane-polarized light image; (**b**) backscattered electron image. The residual fusion crust (FC) enriched in spherical bubbles with different sizes can be found on the margin of images. Pl—plagioclase, Py—pyroxene.

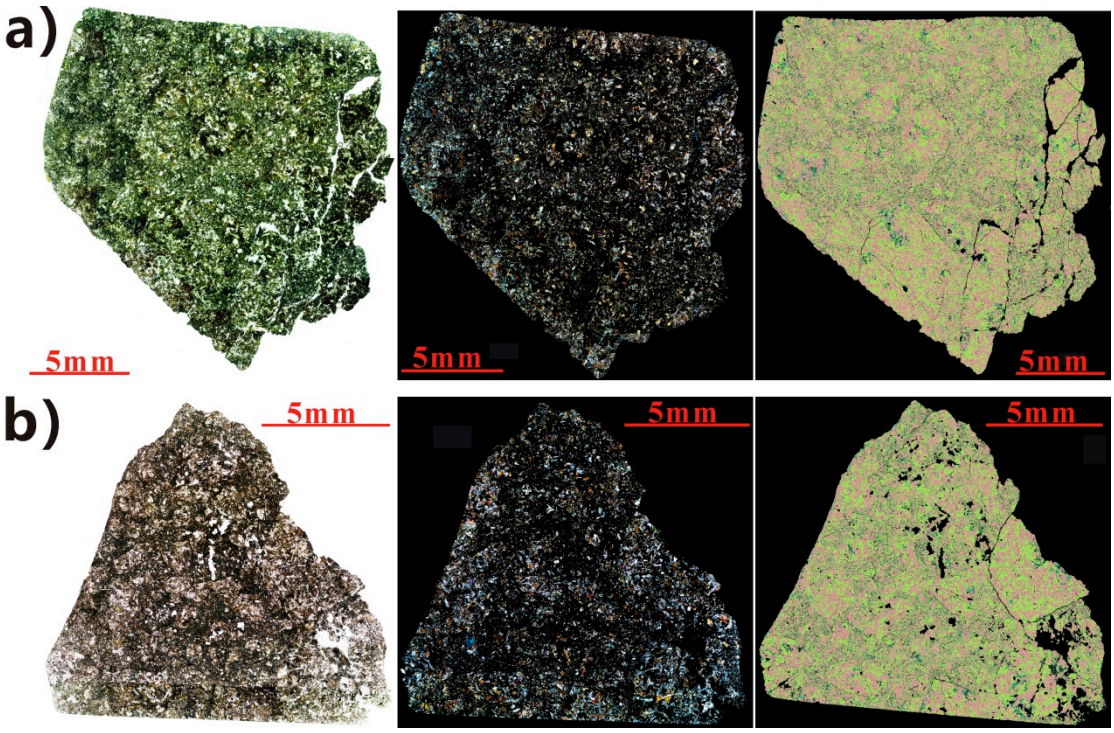


Figure 5. The polished thin sections photos and BSE pseudo color maps of GRV 13001. (**a**) the plane-polarized light image, cross-polarized light image and backscattered electron (BSE) pseudo color map of section A; (**b**) the plane-polarized light image, cross-polarized light image and backscattered electron (BSE) pseudo color map of section B. The photo scales are all 5 mm. The legend in the BSE pseudo color maps is as follows: pink—pyroxene, buff—plagioclase, green—SiO_2, white—opaque mineral, black—cracks or hole. The BSE images are shown in Figure 2.

Finally, the chemical compositions of low-Ca pyroxene, high-Ca pyroxene, and plagioclase in Clast1, Clast1A, Clast2, Clast2A, and Matrix have been obtained by the electron probe microanalysis. The chemical compositions of fusion crust, silica, spinel, and ilmenite are also measured. All the data are listed in Table 1.

3.2. Noble Gases Components

Different noble gas components can be resolved from the measured noble gas data, which thus help to better understand processes associated with these components and timing (ages) associated with such processes. The measured noble gases in meteorites (expressed as subscript "m") are mixtures of a cosmogenic component (expressed as subscript "c"), radiogenic component (expressed as subscript "r"), and trapped component (expressed as subscript "t") [12,13,32]. Usually in meteoritics, cosmogenic noble gases are used to calculate the CRE ages [17], radiogenic noble gases to obtain gas retention ages [33], and trapped noble gases to acquire environmental information of the meteorite parent body [34]. The measured concentrations and isotopic ratios of He, Ne, and Ar of GRV 13001 samples are listed in Table 2.

For helium, the $^{4}He/^{3}He$ ratios of five samples (approximately 195–439) are all significantly lower than the trapped compositions such as solar wind (SW [35]: ~2.2×10^{3}), Earth Air (EA [30]: ~7.1×10^{5}), and Q component (~8.1×10^{3} [34], the trapped or indigenous noble gases in primitive meteorites such as chondrites). Thus, all the ^{3}He concentrations in GRV 13001 samples are assumed to be cosmogenic and we adopt $(^{4}He/^{3}He)_{c} = 5.2$ [36] to subtract the cosmogenic contribution for ^{4}He. For neon, the five samples are dominated by high-energy galactic cosmic rays (GCR) produced cosmogenic Ne (Figure 6), so we derive the $^{21}Ne_{c}$, $(^{20}Ne/^{22}Ne)_{c}$ and $^{20}Ne_{t}$ of samples by mixture-component deconvolutions. We adopt cosmogenic ratio of $(^{20}Ne/^{22}Ne)_{c} = 0.80 \pm 0.03$ [36] and trapped neon ratios of $(^{20}Ne/^{22}Ne)_{t} = 9.8 \pm 0.3$ and $(^{21}Ne/^{22}Ne)_{t} = 0.029 \pm 0.002$ [12,13] to calculate above values. For argon, the measured $^{36}Ar/^{38}Ar$ ratios of the samples (approximately 0.71–0.77) are also closely matching with the cosmogenic ratio $(^{36}Ar/^{38}Ar)_{c}$ (~0.65 [16]). The $^{38}Ar_{c}$ and $^{36}Ar_{t}$ are derived by similar calculation method as for Neon, using a cosmogenic $(^{38}Ar/^{36}Ar)_{c}$ ratio of 1.534 ± 0.047 and a trapped $(^{38}Ar/^{36}Ar)_{t}$ ratio of 0.1885 ± 0.002 [12,13]. All the results are listed in Table 3.

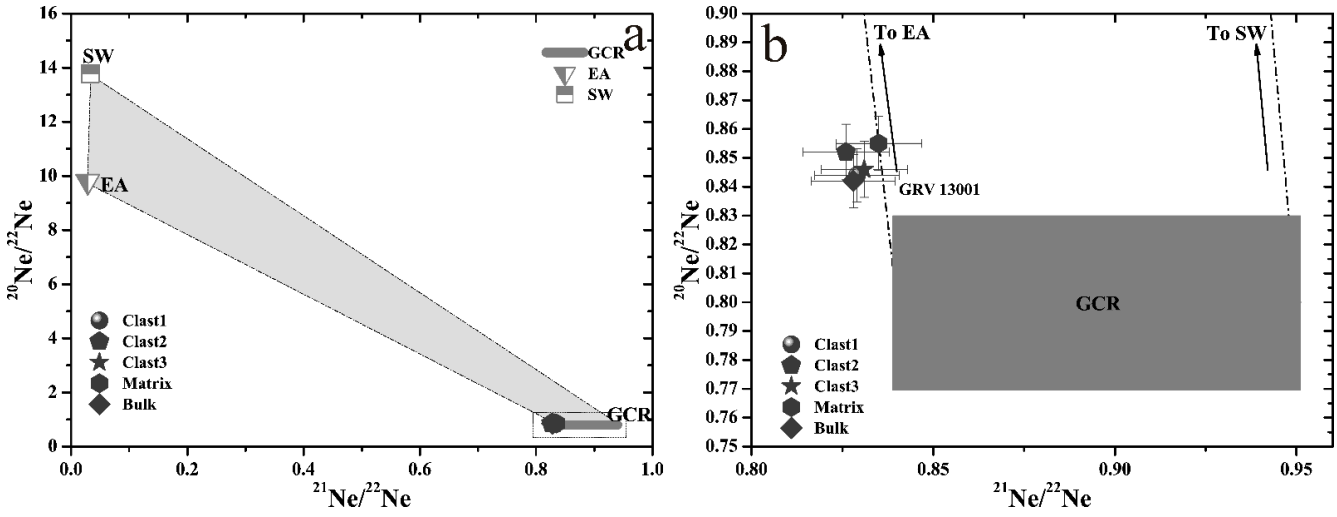


Figure 6. Three-isotope plot of $^{20}Ne/^{22}Ne$ versus $^{21}Ne/^{22}Ne$ ratios of five GRV 13001 samples. The end-member components of solar wind (SW [35]), Earth Air (EA [36]) and cosmogenic Ne produced by high-energy galactic cosmic rays (GCR [12,13,36]) are also plotted. The magnification scale map of the dashed box in (**a**) is given in (**b**).

Table 1. Mineral and fusion crust chemical compositions of GRV 13001 analyzed via electron probe microanalysis (EPMA).

Minerals	**Low-Ca Pyroxene**					**High-Ca Pyroxene**				
Compositions/ wt.%	Clast1 (30)	Clast1A (5)	Clast2 (18)	Clast2A (5)	Matrix (6)	Clast1 (26)	Clast1A (5)	Clast2 (16)	Clast2A (5)	Matrix (8)
SiO_2	49.37	49.97	49.85	50.05	49.18	49.39	49.97	49.82	49.96	49.94
TiO_2	0.23	0.08	0.15	0.11	0.15	0.28	0.34	0.26	0.30	0.24
Al_2O_3	0.20	0.17	0.16	0.10	0.28	0.46	0.41	0.45	0.42	0.42
Cr_2O_3	0.16	0.08	0.08	0.05	0.43	0.52	0.67	0.56	0.58	0.47
FeO	34.66	35.16	34.41	34.72	34.49	24.40	24.01	23.38	22.22	21.18
MnO	1.07	1.07	1.08	1.13	1.05	0.78	0.80	0.74	0.73	0.69
MgO	11.94	12.15	12.11	11.55	11.89	10.56	10.55	10.51	10.29	10.05
CaO	2.22	1.77	2.20	2.42	1.95	13.07	13.18	13.87	15.39	16.41
Na_2O	0.01	0.01	0.01	0.01	0.02	0.03	0.04	0.03	0.02	0.04
Total	99.86	100.46	100.05	100.14	99.44	99.49	99.97	99.62	99.91	99.44
Si	1.978	1.988	1.988	1.997	1.977	1.955	1.964	1.962	1.960	1.964
Ti	0.007	0.002	0.004	0.003	0.004	0.008	0.010	0.008	0.009	0.007
Al	0.009	0.008	0.008	0.004	0.013	0.021	0.019	0.021	0.020	0.020
Cr	0.005	0.002	0.002	0.002	0.014	0.016	0.021	0.018	0.018	0.015
Fe	1.161	1.170	1.147	1.159	1.160	0.809	0.791	0.771	0.730	0.698
Mn	0.036	0.036	0.037	0.038	0.036	0.026	0.027	0.025	0.024	0.023
Mg	0.713	0.720	0.720	0.687	0.713	0.623	0.619	0.617	0.602	0.589
Ca	0.095	0.075	0.094	0.103	0.084	0.554	0.553	0.584	0.645	0.690
Na	0.001	0.001	0.001	0.001	0.001	0.002	0.003	0.002	0.002	0.003
Total	4.005	4.002	4.001	3.994	4.002	4.014	4.007	4.008	4.010	4.009
Fs/mol.%	59.0 ± 1.4	59.5 ± 1.2	58.5 ± 1.1	59.5 ± 0.5	59.3 ± 0.7	40.7 ± 5.6	40.3 ± 7.8	39.1 ± 5.9	37.0 ± 7.2	35.3 ± 8.0
Wo/mol.%	4.8 ± 2.0	3.8 ± 1.3	4.8 ± 1.9	5.3 ± 0.4	4.3 ± 0.9	27.9 ± 6.6	28.2 ± 9.3	29.6 ± 7.2	32.6 ± 8.5	34.9 ± 9.3
En/mol.%	36.2 ± 1.2	36.7 ± 0.7	36.7 ± 1.1	35.2 ± 0.3	36.4 ± 0.8	31.4 ± 1.1	31.5 ± 1.9	31.3 ± 1.3	30.4 ± 1.3	29.8 ± 1.4
$Mg^{\#}$/mol.%	38.0 ± 0.9	38.1 ± 0.7	38.6 ± 0.7	37.2 ± 0.4	38.1 ± 0.7	43.8 ± 2.9	44.3 ± 4.0	44.7 ± 3.1	45.5 ± 3.7	46.3 ± 4.4
Fe/Mn	32.1 ± 2.9	32.5 ± 2.5	31.5 ± 2.7	30.3 ± 1.4	32.7 ± 4.0	31.3 ± 3.7	29.8 ± 1.4	31.5 ± 3.6	30.4 ± 2.9	30.3 ± 4.7

Minerals	Plagioclase					Spinel	Ilmenite	Silica	Fusion crust	
Compositions/ wt.%	Clast1 (18)	Clast1A (5)	Clast2 (15)	Clast2A (4)	Matrix (9)	(7)	(9)	(27)	(26)	
SiO_2	46.62	46.63	47.14	46.25	47.68	0.05	0.07	98.37		48.78
TiO_2	n.d.	n.d.	n.d.	n.d.	n.d.	5.39	53.21	0.07		0.59
Al_2O_3	32.74	32.69	32.47	32.72	32.29	8.02	n.d.	0.54		12.17
Cr_2O_3	n.d.	n.d.	n.d.	n.d.	n.d.	48.68	0.40	0.15		0.42
V_2O_3	n.d.	n.d.	n.d.	n.d.	n.d.	0.64	n.d.	n.d.		n.d.
FeO	0.52	0.63	0.46	0.56	0.75	35.72	44.79	0.53		19.88
MnO	n.d.	n.d.	n.d.	n.d.	n.d.	0.50	0.92	n.d.		0.65
MgO	0.11	0.11	0.10	0.13	0.06	0.85	0.94	n.d.		6.43
CaO	17.88	17.81	17.82	18.13	17.23	0.11	0.27	0.26		9.88
Na_2O	1.11	1.12	1.14	0.99	1.35	n.d.	n.d.	n.d.		0.39
K_2O	0.08	0.07	0.08	0.06	0.11	n.d.	n.d.	n.d.		n.d.
Total	99.06	99.06	99.21	98.86	99.47	99.96	100.60	99.92		99.19
Si	2.166	2.168	2.185	2.156	2.203	0.002	0.002			
Ti	n.d.	n.d.	n.d.	n.d.	n.d.	0.144	0.990			
Al	1.794	1.791	1.773	1.798	1.758	0.336	n.d.			
Cr	n.d.	n.d.	n.d.	n.d.	n.d.	1.367	0.008			
V	n.d.	n.d.	n.d.	n.d.	n.d.	0.018	n.d.			
Fe	0.020	0.025	0.018	0.022	0.029	1.061	0.926			
Mn	n.d.	n.d.	n.d.	n.d.	n.d.	0.015	0.019			
Mg	0.007	0.008	0.007	0.009	0.004	0.045	0.034			
Ca	0.890	0.888	0.885	0.906	0.853	0.004	0.007			
Na	0.100	0.101	0.102	0.090	0.121	n.d.	n.d.			
K	0.005	0.004	0.004	0.004	0.006	n.d.	n.d.			
Total	4.982	4.985	4.974	4.985	4.974	2.992	1.986			
An/mol.%	89.5 ± 4.2	89.4 ± 4.7	89.2 ± 3.5	90.6 ± 1.2	86.9 ± 6.5					
Or/mol.%	0.5 ± 0.3	0.4 ± 0.3	0.5 ± 0.3	0.4 ± 0.1	0.7 ± 0.4				$Mg^{\#}$/mol.%	63.3 ± 3.0
Ab/mol.%	10.0 ± 3.9	10.2 ± 4.5	10.3 ± 3.2	9.0 ± 1.2	12.4 ± 6.2				Fe/Mn	30.4 ± 4.0

Note: (1) Values in parentheses represent number of analysis points. (2) n.d.—not detected or low than the detection limits of the EPMA. (3) $Mg^{\#}$ = Mg / (Fe + Mg) ×100%

Table 2. Results of He, Ne, and Ar measurements for GRV 13001.

Sample	**Weight/mg**	$^{4}He_m$	$(^{4}He/^{3}He)_m$	$^{22}Ne_m$	$(^{20}Ne/^{22}Ne)_m$	$(^{21}Ne/^{22}Ne)_m$	$^{40}Ar_m$	$(^{40}Ar/^{36}Ar)_m$	$(^{36}Ar/^{38}Ar)_m$
Bulk	2.3	8940 ± 171	260 ± 4	6.22 ± 0.04	0.842 ± 0.009	0.828 ± 0.012	1789 ± 37	782 ± 24	0.74 ± 0.02
Matrix	2.33	7593 ± 146	229 ± 3	5.63 ± 0.03	0.855 ± 0.009	0.835 ± 0.012	1784 ± 39	746 ± 24	0.77 ± 0.03
Clast3	0.94	7591 ± 145	196 ± 3	6.31 ± 0.04	0.846 ± 0.010	0.831 ± 0.012	1823 ± 40	793 ± 25	0.71 ± 0.02
Clast2	0.87	14,706 ± 281	439 ± 7	6.09 ± 0.04	0.852 ± 0.010	0.826 ± 0.012	2381 ± 52	923 ± 29	0.72 ± 0.02
Clast1	3.76	7864 ± 150	213 ± 3	6.58 ± 0.04	0.844 ± 0.009	0.829 ± 0.012	2122 ± 47	836 ± 6	0.71 ± 0.01

Note: Concentrations are given in 10^{-8} ccSTP/g.

Table 3. Concentrations of cosmogenic (c), trapped (t), radiogenic (r) He, Ne, and Ar of GRV 13001 samples, and their CRE and gas retention ages.

Sample	$^{3}He_c$	$^{4}He_r$	$(^{22}Ne/^{21}Ne)_c$	$^{21}Ne_c$	$^{20}Ne_t$	$^{38}Ar_c$	$^{36}Ar_t$	T_3/Ma	T_{21}/Ma	T_{38}/Ma	T_4/Ga	T_{40}/Ga
Bulk	34.4 ± 0.8	8761 ± 171	1.202± 0.018	5.15 ± 0.07	0.29 ± 0.20	3.05 ± 0.07	0.30 ± 0.07	21.4 ± 2.2	30.3 ± 3.1	20.3 ± 4.1	~2.9	~3.7
Matrix	33.1 ± 0.8	7421 ± 146	1.191± 0.017	4.70 ± 0.06	0.33 ± 0.17	3.04 ± 0.07	0.41 ± 0.08	20.6 ± 2.1	27.0 ± 2.7	20.3 ± 4.1	~2.5	~3.6
Clast3	38.8 ± 0.9	7389 ± 145	1.196± 0.018	5.25 ± 0.07	0.32 ± 0.20	3.20 ± 0.08	0.21 ± 0.07	24.1 ± 2.5	30.5 ± 3.0	21.3 ± 4.3	~2.5	~3.7
Clast2	33.5 ± 0.8	14,532 ± 281	1.204± 0.017	5.03 ± 0.06	0.35 ± 0.19	3.55 ± 0.08	0.27 ± 0.08	20.9 ± 2.1	29.6 ± 3.0	23.7 ± 4.8	~4.0	~4.1
Clast1	36.9 ± 0.9	7672 ± 150	1.199± 0.017	5.46 ± 0.07	0.31 ± 0.21	3.53 ± 0.08	0.24 ± 0.08	23.0 ± 2.4	31.9 ± 3.2	23.5 ± 4.7	~2.6	~3.9

Note: (1) Concentrations are given in 10^{-8} ccSTP/g; (2) T_3—the CRE age calculated based on cosmogenic ^{3}He and its production rate, T_{21}—the CRE age calculated based on cosmogenic ^{21}Ne and its production rate, T_{38}—the CRE age calculated based on cosmogenic ^{38}Ar and its production rate; (3) We adopt the T_{21} ages to the preferred CRE ages of analyzed samples, see Section 4.2.2 for detail discussion; (4) T_4—the U,Th-^{4}He nominal gas retention ages calculated based on radiogenic ^{4}He and the content of U and Th elements, T_{40}—the ^{40}K-^{40}Ar nominal gas retention ages calculated based on radiogenic ^{40}Ar and the content of K element; (5) The errors in the T_4 and T_{40} ages do not include the content errors of U, Th and K.

4. Discussion

4.1. Meteorite Classification

Chen et al. (2015) [23] briefly reported the petrologic characteristics of GRV 13001 and classified it as a monomict eucrite. GRV 13001 has an ophitic/subophitic texture consisting of mainly pyroxene, plagioclase, a few silica phases, and sporadic zircons along with a residual fusion crust. At present, the extraterrestrial magmatic rocks in our collection primarily include Martian meteorites, lunar samples, HEDs, angrites, ureilites, and iron meteorites [10]. Since these rocks formed in different crystallization environments under ranges of pressures, temperatures, and oxygen fugacity, their main crystalline minerals (such as pyroxene and feldspar) have distinct chemical compositions [37]. According to these characteristics, different types of igneous differentiated meteorites or rocks can be distinguished from each other. The Fe/Mn ratios of pyroxenes in Sections A and B of GRV 13001 are 31.6 ± 3.5 and 31.3 ± 2.9, respectively, and the An values (mol. %) of plagioclases are 88.7 ± 4.9 and 89.5 ± 3.7, respectively. They all completely fall into the pyroxenes Fe/Mn area (30 ± 2) and plagioclases An range (87 ± 2) of HEDs (Figure 7a), respectively. Additionally, the MnO vs. FeO/MnO of pyroxenes of GRV 13001 also fall within the HED region (Figure 7b).

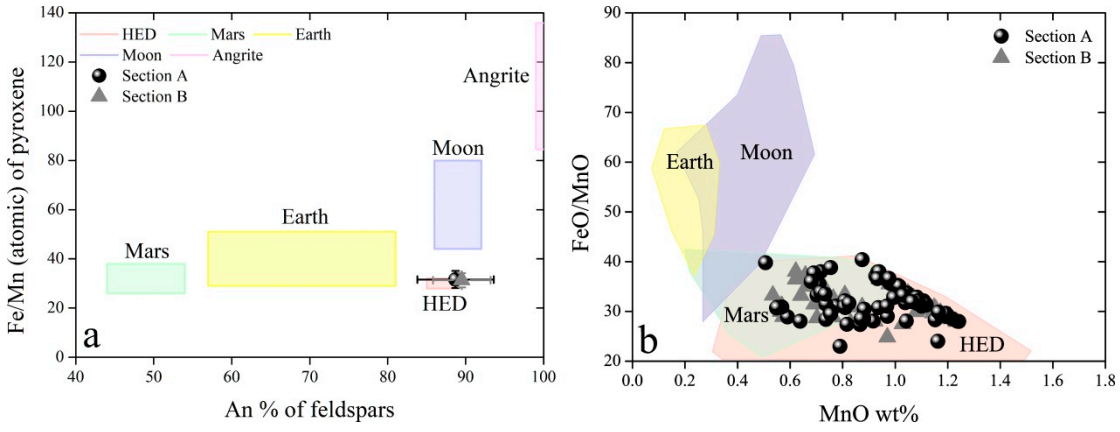


Figure 7. Comparison of the minerals chemical compositions of terrestrial rocks, Martian, lunar, Howardite-Eucrite-Diogenites (HEDs), angrite meteorites and GRV 13001 (Section A and B). Literature data are from [2,38–40]. (**a**) An% of feldspars vs. Fe/Mn of pyroxene, (**b**) FeO/MnO vs. MnO of pyroxene. The data of GRV 13001 fall within the HED region.

The eucrites can be subdivided into plutonic cumulate eucrites and hypabyssal/extrusive basaltic eucrites [1,2]. Due to differences in crystallization conditions between diogenites and cumulate/basaltic eucrites, the compositions of mafic minerals (e.g., low-

Ca pyroxenes) and opaque minerals (e.g., ilmenite) gradually change from Mg-rich to Fe-rich. The $Mg^{\#}$ number (Mg/(Mg + Fe) mol.%) reflect well the compositional variation of low-Ca pyroxenes, which shows transition from 68 to 72 mol.% diogenites, to 50–65 mol.% cumulate eucrites and eventually to 32–45 mol.% basaltic eucrites [2]. The $Mg^{\#}$ number and chemical compositions of pyroxenes in GRV 13001 are 36–40 mol.% and $Fs_{58.9\pm1.2}Wo_{4.7\pm1.8}En_{36.3\pm1.1}$ to $Fs_{39.2\pm6.4}Wo_{29.7\pm7.7}En_{31.1\pm1.4}$, respectively, which fall within the basaltic eucrites range (Figure 8a,b). Similarly, the compositions of ilmenites in GRV 13001 are also Fe-rich and fall within the basaltic eucrite range (Figure 8c).

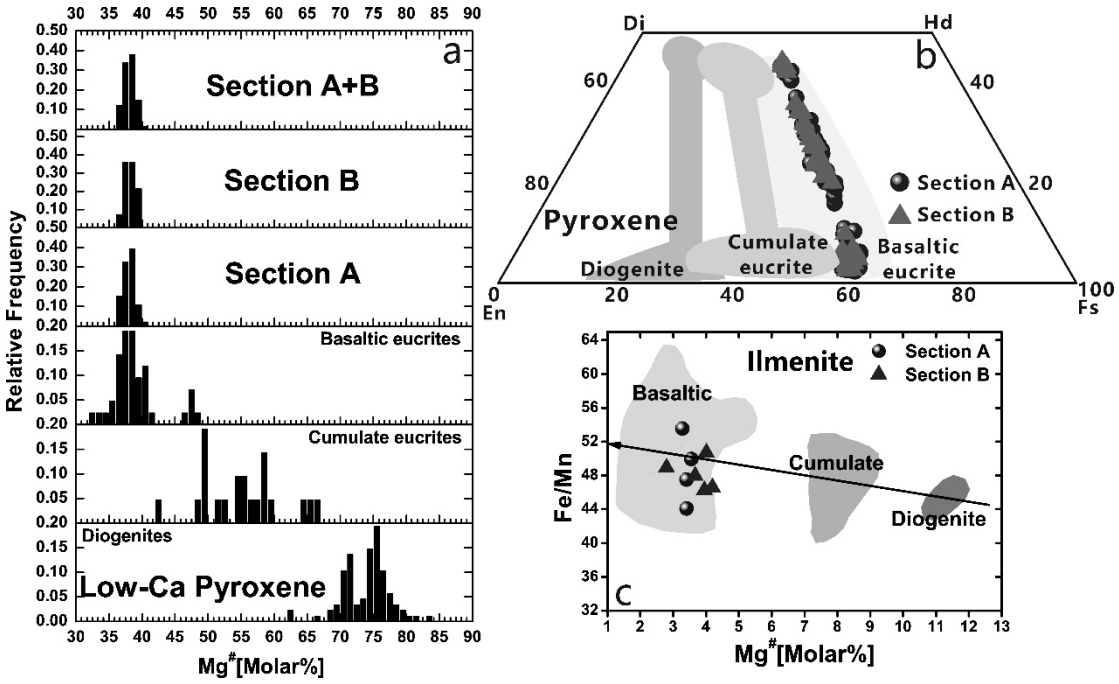


Figure 8. Comparison of minerals chemical compositions of HED meteorites and GRV 13001 (Section A and B). The compositions of HEDs are from [2]. (**a**) low-Ca pyroxene, (**b**) pyroxene, (**c**) ilmenite. GRV 13001 falls within the basaltic eucrite range.

The measurements from the electron probe microanalysis indicate that the chemical compositions of the same species of minerals in Clast1, Clast1A, Clast2, Clast2A, and Matrix are almost consistent (Table 1). Chemical compositions of GRV 13001 fusion crust are similar to the average bulk compositions of monomict basaltic eucrites (Table 4). Further, the clasts in GRV 13001 have same ophitic/subophitic texture, and the mineral assemblage of clasts and matrix are also consistent. Consequently, this meteorite is indeed a brecciated monomict basaltic eucrite as shown in previous preliminary work [23].

Table 4. Comparisons between the chemical compositions of GRV 13001 fusion crust and the average bulk compositions of monomict basaltic eucrites.

wt.%	Na	Mg	Al	Si	Ca	Fe	Ti	Cr	Mn	S	Ni	K/ppm	U/ppb	Th/ppb
Fusion Crust (FC)	0.29	3.88	6.43	22.80	7.15	15.25	0.36	0.24	0.50	n.d.	n.d.	n.d.	n.d.	n.d.
Average (Monomict Basaltic Eucrites)	0.31	4.20	6.60	22.90	7.30	14.90	0.43	0.23	0.43	0.20	6.7×10^{-4}	389	114	356
FC/av. (%)	94	92	97	100	98	102	84	106	117					

Note: (1) n.d.—not detected or low than the detection limits; (2) The average (av.) chemical compositions of 35 monomict basaltic eucrites are calculated based on the data from [2].

4.2. Noble Gas Concentrations, Ratios and Ages

4.2.1. Evidence for Solar-Derived Noble Gases?

Although the noble gases in meteorites are a mixture of many components, they can be distinguished and analyzed using isotope ratios (mainly neon three-isotope plot [13]). For example, the solar wind has a high $^{20}Ne/^{22}Ne$ ratio and a low $^{21}Ne/^{22}Ne$ ratio [35], while the cosmogenic Ne has the significantly different isotopic ratios [12]. In addition, meteoroids are affected by two kinds of cosmic rays in space, namely high-energy galactic cosmic rays (GCR) and low-energy solar cosmic rays (SCR) [17]. The penetration depth of the former can reach more than 1 m, while the latter is less than 2 cm [12,41]. Because the surface material of meteorite is ablated during atmospheric entry to the Earth, and the noble gas produced by SCR component is unlikely to survive the process [13], especially for the large meteorites. Thus, we assume that the contribution of SCR to the cosmogenic noble gas budget of GRV 13001 is negligible.

Figure 6 is a Ne three-isotope plot of $^{20}Ne/^{22}Ne$ versus $^{21}Ne/^{22}Ne$ ratios for all the five GRV 13001 samples, obtained through laser-heating, and literature values are also given for the $^{20}Ne/^{22}Ne$ versus $^{21}Ne/^{22}Ne$ ratios of end-member components of solar wind (SW), Earth Air (EA) and cosmogenic Ne produced by high-energy galactic cosmic rays (GCR). The gray band (Figure 6) is the typical range of HEDs showing mixing between SW, EA, and GCR components. Overall, the neon compositions of the GRV 13001 samples are dominated by GCR produced cosmogenic Ne (Figure 6), which supports the above assumption that the effect of SCR produced Ne in GRV 13001 is negligible.

Finally, the elemental ratio $^{4}He/^{20}Ne_t$ of GRV 13001 approximately range from 2.3×10^4 to 4.2×10^4, which are much higher than those of solar wind (~650 [35]), Earth Air (~0.32 [30]) and planetary-rich components (~110 [34]). It indicates that almost all ^{4}He in GRV 13001 is radiogenic. Similarly, $^{40}Ar/^{36}Ar$ ratios of GRV 13001 (~750 to 920) are also much larger than those of lunar soils (~0 to 16 [42]) and planetary-rich components (<0.12 [34]). In addition, the low $^{36}Ar_t$ concentrations of GRV 13001 (Table 3) also rule out any significant contribution of earth air to the ^{40}Ar abundance of this meteorite. This suggests that the ^{40}Ar in GRV 13001 is also mainly radiogenic. As a consequence, the ^{4}He and ^{40}Ar of this meteorite can be safely used to calculate the nominal gas retention ages.

4.2.2. Cosmic-Ray Exposure (CRE) Ages

During the period of exposure to high energy cosmic-ray, meteorites will produce cosmogenic nuclides. Based on the concentrations (C) and production rates (P) of cosmogenic stable isotopes (^{3}He, ^{21}Ne, ^{38}Ar, etc.), we can calculate the time at which a meteorite began to be exposed to cosmic rays, i.e., the CRE age (=C/P), which represents the transitory exposure time of the meteorite in space or its ejection event from the parent body [15–17]. Eugster and Michel [36] successfully derived the production rates of cosmogenic ^{3}He, ^{21}Ne, and ^{38}Ar for HED meteorites, which are now the most widely used. Briefly, the production rates (P') was first obtained from the chemical compositions of analyzed samples, and then, the actual production rates (P) can be acquired from the empirical relationships between the shielding indicator $(^{22}Ne/^{21}Ne)c$ and burial depth of samples.

Based on the measured concentrations of cosmogenic ^{3}He, ^{21}Ne and ^{38}Ar (Table 3), we focus on the production rates (P_3, P_{21}, and P_{38}) of ^{3}He, ^{21}Ne, and ^{38}Ar to accurately calculate the CRE ages (T_3, T_{21}, and T_{38}) of GRV 13001. GRV 13001 is a monomict basaltic eucrite with homogeneous minerals chemical compositions, so the analyzed samples can be approximated as mixtures of main minerals (pyroxene and plagioclase) with different mixing ratios. Here, we adopt the chemical compositions of the low-Ca pyroxene (Low Ca), high-Ca pyroxene (High Ca) and plagioclase (Pl) of Clast1 to calculate the production rates respectively, and the chemical compositions of GRV 13001 fusion crust (FC) and monomict basaltic eucrites (Eucrite) are also added for comparison. A similar operation is then performed on the Clast2 and Matrix samples, while the Bulk sample is compared using only the compositions of latter two components (FC and Eucrite).

Regardless of which components are adopted to calculate the production rates, the P_{21} values of the Clast1, Clast2, and Matrix samples are always consistent, and so are P_3, but the P_{38} vary widely (Figure 9). P_3 and P_{21} have no correlation with the chemical compositions used in the calculation, indicating that the $^{3}He_c$ and $^{21}Ne_c$ production rates of GRV 13001 are almost unaffected by the changes in the mineral compositions of the analyzed samples. The apparent difference for P_{38} is because the $^{38}Ar_c$ in meteorites is mainly produced by the interaction of calcium with cosmic rays [43,44]. Thus, the mixing ratios of low-Ca pyroxene, high-Ca pyroxene, and plagioclase seriously affect the total calcium abundances within the analyzed samples. This, in turn, affects the calculation of P_{38}. The Bulk sample has a similar trend except for P_{38}, which is due to the consistent calcium contents of GRV 13001 fusion crust and average monomict basaltic eucrites (Table 4).

On the other hand, the lower closure temperature of ^{3}He (<100 °C) leads to easier loss of ^{3}He by solar heating or impact events, resulting in the generally underestimated T_3 ages of meteorites [45,46]. Moreover, ^{36}Cl produced by a neutron capture reaction [47,48] and the terrestrial weathering [49,50] increase the uncertainty of T_{38} ages of meteorites. Therefore, there is a general consensus that the T_{21} age is more reliable than the T_3 age and T_{38} age, and the T_{21} age represents the CRE age of meteorites [14,17,46]. After consideration of measurement conditions, experimental constraints and CRE age accuracy, the chemical compositions of the fusion crust are adopted to calculate the production rates of GRV 13001 meteorite in the following sections.

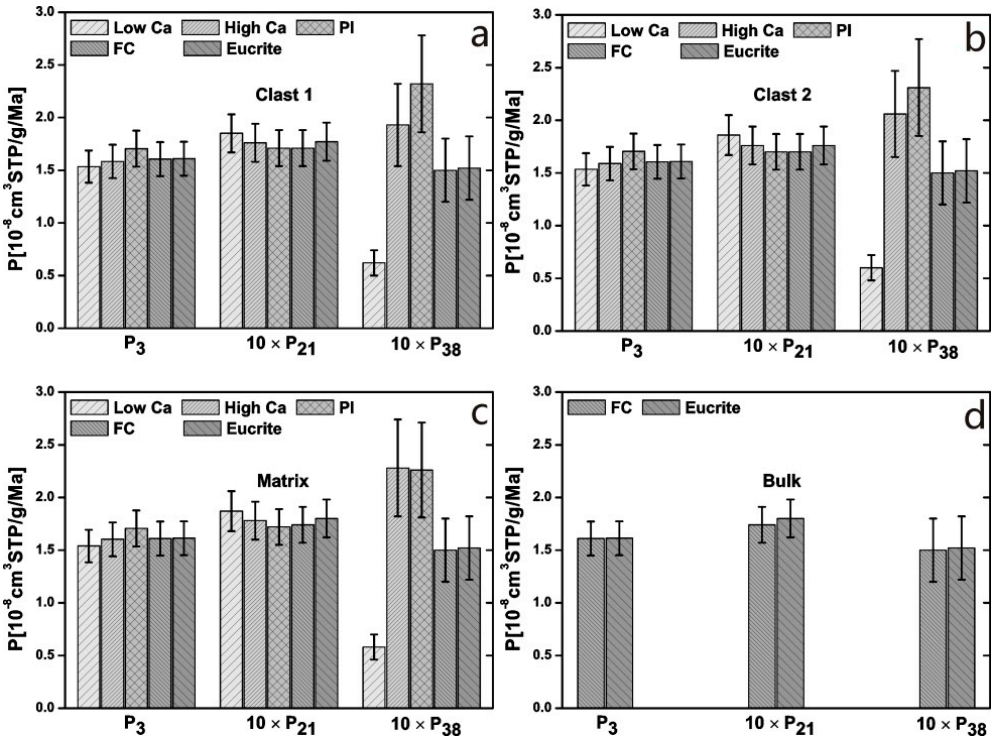


Figure 9. The production rates of cosmogenic ^{3}He, ^{21}Ne, and ^{38}Ar of Clast1 (**a**) are compared using chemical compositions of different main minerals and components. Similar operations are then performed on the Clast2 (**b**), Matrix (**c**) and Bulk (**d**) samples. The Eugster and Michel [36] model is adopted to calculate the production rates. Abbreviations: Low Ca—low calcium pyroxene, High Ca—high calcium pyroxene, Pl—plagioclase, FC—fusion crust, Eucrite—average bulk compositions of monomict basaltic eucrites. The $^{3}He_c$ and $^{21}Ne_c$ production rates of GRV 13001 are almost unaffected by the changes in the mineral compositions of the analyzed samples, but the production rates of $^{38}Ar_c$ are mainly dependent on the calcium contents of the analyzed samples.

Here we adopt the T_{21} ages calculated using the Eugster model as the final CRE ages of analyzed samples, and the T_3 and T_{38} ages are also calculated for comparison (Table 3).

The preferred CRE ages of the Bulk, Matrix, Clast3, Clast2, and Clast1 are 30.3 ± 3.1 Ma, 27.0 ± 2.7 Ma, 30.5 ± 3.0 Ma, 29.6 ± 3.0 Ma, and 31.9 ± 3.2 Ma, respectively, which are consistent within the error range (Table 3). Averaging the value of all five samples results in a final CRE age of GRV 13001 eucrite of 29.9 ± 3.0 Ma.

4.2.3. Nominal Gas Retention Ages

After the meteorites formation and the cooling process below the closure temperatures of ^{4}He and ^{40}Ar, the radiogenic $^{4}He_{r}$ (U,Th decay) and $^{40}Ar_{r}$ (^{40}K decay) begin to accumulate, allowing the determination of U,Th-^{4}He (T_4) and ^{40}K-^{40}Ar (T_{40}) gas retention ages. However, subsequent late thermal events, such as strong impacts, can reset these dating systems [21]. Here, we adopt the average contents of U, Th, and K of monomict basaltic eucrites (Table 4) to calculate the nominal gas retention ages T_4 and T_{40} (Table 3). The T_4 ages of the Bulk, Matrix, Clast3, Clast2, and Clast1 samples of the eucrite GRV 13001 are approximately 2.9 Ga, 2.5 Ga, 2.5 Ga, 4.0 Ga, and 2.6 Ga, respectively. On the other hand, the T_4 ages of those samples are less than the corresponding T_{40} ages, which are approximately 3.7 Ga, 3.6 Ga, 3.7 Ga, 4.1 Ga, and 3.9 Ga for the Bulk, Matrix, Clast3, Clast2, and Clast1 samples, respectively.

4.3. The Exposure and Impact/Thermal Histories of GRV 13001

The CRE ages distributions of HED meteorites exhibit common clusters, which suggest the ejection events of HEDs were caused by large impacts on the HED parent body [36]. At present, it is generally believed that the CRE ages of HEDs have two peaks at 17–23 Ma and 35–41 Ma without considering the meteorite types [12], indicating two major impact events of the parent body occurred at ~20 Ma and 40 Ma [17]. The two large impact events liberated approximately more than one third of collected HEDs [15]. In addition, there are at least 5–10 other impact events to explain the CRE age distribution of the remaining HED meteorites [12].

The HED polymict breccias and howardites have complex materials sources and formation mechanisms [2], which greatly affect the reliability and interpretation of CRE ages of meteorites [13]. Here, we compile currently published T_{21} ages of unbrecciated and monomict eucrites, unbrecciated, and monomict diogenites, and all types of HEDs (Figure 10) to readdress and verify possible ejection events by identifying the T_{21} ages clusters of these meteorites. More than 99% impact events occurred at HED parent body have <10 km/s impact velocity [51], corresponding to <6 km excavation depth [22]. However, diogenite is formed at >20 km below the surface of HED parent body [2,52]. Thus, weak ejection events can only launch eucrite and howardites, which are located at shallower depths of HED parent body. Whereas, diogenite can be ejected from HED parent body only by large impact events, which also launch exterior eucrites and howardites simultaneously [36]. Consequently, the distributions of T_{21} ages of unbrecciated and monomict diogenites may indicate at least four large impact evens (Figure 10). Meanwhile, the eucrites (unbrecciated and monomict) and all types of HEDs indeed have T_{21} age clusters similar to those of the diogenites, i.e., 7.5–15.0 Ma, 17.5–25.0 Ma, 35.0–42.5 Ma, and 55.0–60.0 Ma. As a consequence, if Vesta is assumed to be the main ejection source of HED meteorites [18], the T_{21} age distributions indicate that there are at least four major impact events or periods on Vesta, and more than 70% of HEDs are launched by these events. Finally, the CRE age of GRV 13001 is within the typical range of approximately 5–60 Ma of HED meteorites (Figure 10), but significantly deviates from these major impact events.

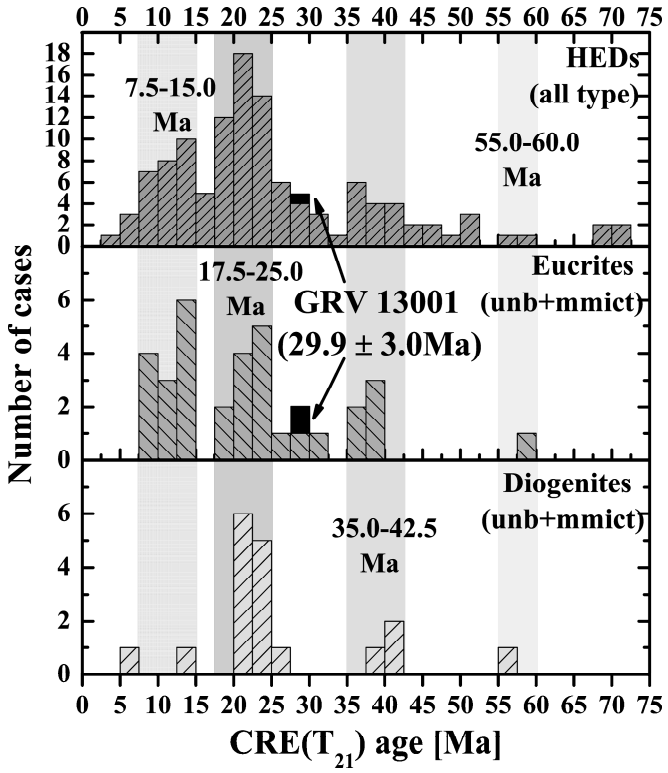


Figure 10. CRE (T_{21}) ages histograms of all HED meteorites, unbrecciated (unb) and monomict (mmict) eucrites, unbrecciated and monomict diogenites. Literature data are from [15,17,18,36]. The petrographic types of meteorites are according to [2]. There are at least four major impact events or periods (gray boxes), and more than 70% of HEDs are launched by these events. GRV 13001 deviates from these events.

The T_{40} ages of GRV 13001 (~3.6 to 4.1 Ga) are less than the crystallization ages of eucrites (~4.55 Ga) [1,2], which indicates that the ^{40}K–^{40}Ar system of the meteorite have been reset due to subsequent thermal events. Additionally, the T_4 ages (2.9 Ga, 2.5 Ga, 2.5 Ga, 4.0 Ga, and 2.6 Ga) are less than the T_{40} ages (3.7 Ga, 3.6 Ga, 3.7 Ga, 4.1 Ga, and 3.9 Ga) of the Bulk, Matrix, Clast3, Clast2, and Clast1 samples. This is mainly due to the lower closure temperature of ^{4}He, which is more susceptible to diffusion loss than ^{40}Ar. Although there is no strict geological significance for the T_{40} gas retention age, it still implies that the GRV 13001 eucrite was likely to have been subjected to intense thermal processes during ~3.6 Ga to 4.1 Ga. Actually, the ^{40}Ar-^{39}Ar age studies of the HED meteorites do find that their parent body is likely to experience K-Ar reset events caused by intense impacts at ~3.45 to 3.55 Ga and ~3.9 to 4.0 Ga, respectively [21,22]. This to some extent supports the speculation that the GRV 13001 experienced intense impact processes during brecciation.

In addition, it is noted that the Clast1, Clast3, and Matrix samples have self-consistent T_4 nominal gas retention ages (~2.5 to 2.6 Ga), which we suspect may represent a weak thermal event experienced by the meteoroid. The radiogenic ^{4}He has been lost during this process, but the thermal strength is not sufficient to reset the K–Ar system. Eugster et al. (2007) [32] used the age ratios of T_3/T_{21} vs. T_4/T_{40} to analyze the radiogenic ^{4}He loss of chondrites and argue that if the age ratios of meteorites follow the trend line with a slope of one, it indicates that the cosmogenic ^{3}He and radiogenic ^{4}He of the meteorites have been lost during their cosmic ray exposure. Conversely, if the meteorites have concordant T_3 and T_{21} ages, the radiogenic ^{4}He should be lost before their cosmic ray exposure. The $(T_4/T_{40})/(T_3/T_{21})$ of Bulk, Matrix, Clast3, and Clast1 samples are 1.1, 0.9, 0.9, and 0.9, respectively, which are all following the trend line of a slope of one. This likely indicates the cosmogenic ^{3}He and radiogenic ^{4}He of GRV 13001 was not well-retained during their subsequent cosmic ray exposure history. Thus, the above mentioned weak thermal event

experienced by the GRV 13001 occurs after the ejection event (~30 Ma) of this meteorite from its parent body. Furthermore, the He loss may be caused by solar heating [45,53], which results from the smaller heliocentric distance before GRV 13001 approached Earth.

5. Conclusions

1. GRV13001 is a monomict basaltic eucrite with typical ophitic/subophitic texture and residual fusion crust, consists mainly of low-Ca pyroxene and plagioclase, which have normal eucritic chemical compositions. The Bulk, matrix and three clasts samples of the GRV 13001 have almost similar CRE ages of approximately 29.9 ± 3.0 Ma. Moreover, its U,Th-^{4}He and ^{40}K-^{40}Ar gas retention ages are ~2.6 to 3.9 Ga and ~3.6 to 4.1 Ga, respectively.
2. Based on the currently published T_{21} ages of HED meteorites, it is suggested that there are at least four major impact events or periods on the HED parent body, i.e., 7.5–15.0 Ma, 17.5–25.0 Ma, 35.0–42.5 Ma, and 55.0–60.0 Ma, and more than 70% of HEDs are launched by these events. The CRE age of the GRV 13001 significantly deviates from these major impact events. Finally, the nominal T_{40} gas retention ages may imply that the GRV 13001 experienced intense impact processes during brecciation. Further, it may have also experienced weak thermal event after the ejection event of this meteorite at ~30 Ma.

Author Contributions: Writing—original draft preparation, C.Z.; writing—review and editing, B.M.; noble gases data curation, H.H. and P.M.R.; petrology and chemical compositions data curation, H.C. and Q.X. All authors have read and agreed to the published version of the manuscript.

Funding: This research was funded by Strategic Priority Research Program of Chinese Academy of Sciences (XDB 41000000), Project funded by China Postdoctoral Science Foundation (2020M673557XB), Civil Aerospace Pre Research Project (D020302 and D020206), Foundation of Guilin University of Technology (GUTQDJJ2019165), and the grant from Key Laboratory of Lunar and Deep Space Exploration, CAS (LDSE201907).

Data Availability Statement: This work did not report any data.

Acknowledgments: We thank Polar Research Institute of China and Resource-sharing Platform of Polar Samples for allocation of the GRV 13001 samples. Additionally, we thank three anonymous reviewers and editors for their helpful comments and suggestions.

Conflicts of Interest: The authors declare no conflict of interest.

References

1. McSween, H.Y.; De Sanctis, M.C.; Prettyman, T.H. Unique, Antique Vesta. *Elements* **2014**, *10*, 39–44. [CrossRef]
2. Mittlefehldt, D.W. Asteroid (4) Vesta: I. The howardite-eucrite-diogenite (HED) clan of meteorites. *Chem. der Erde-Geochem.* **2015**, *75*, 155–183. [CrossRef]
3. Mccord, T.B.; Adams, J.B.; Johnson, T.V. Asteroid Vesta: Spectral Reflectivity and Compositional Implications. *Science* **1970**, *168*, 1445–1447. [CrossRef] [PubMed]
4. Marchi, S.; McSween, H.Y.; O'Brien, D.P.; Schenk, P.; De Sanctis, M.C.; Gaskell, R.; Jaumann, R.; Mottola, S.; Preusker, F.; Raymond, C.A.; et al. The Violent Collisional History of Asteroid 4 Vesta. *Science* **2012**, *336*, 690–694. [CrossRef]
5. Binzel, R.P.; Xu, S. Chips off of Asteroid 4 Vesta: Evidence for the Parent Body of Basaltic Achondrite Meteorites. *Science* **1993**, *260*, 186–191. [CrossRef] [PubMed]
6. Greenwood, R.C.; Burbine, T.H.; Miller, M.F.; Franchi, I.A. Melting and differentiation of early-formed asteroids: The perspective from high precision oxygen isotope studies. *Chem. der Erde-Geochem.* **2017**, *77*, 1–43. [CrossRef]
7. Scott, E.R.; Greenwood, R.C.; Franchi, I.A.; Sanders, I.S. Oxygen isotopic constraints on the origin and parent bodies of eucrites, diogenites, and howardites. *Geochim. Cosmochim. Acta* **2009**, *73*, 5835–5853. [CrossRef]
8. Yamaguchi, A.; Clayton, R.N.; Mayeda, T.K.; Ebihara, M.; Oura, Y.; Miura, Y.N.; Haramura, H.; Misawa, K.; Kojima, H.; Nagao, K. A New Source of Basaltic Meteorites Inferred from Northwest Africa 011. *Science* **2002**, *296*, 334–336. [CrossRef] [PubMed]
9. Zhang, C.; Miao, B.; He, H. Oxygen isotopes in HED meteorites and their constraints on parent asteroids. *Planet. Space Sci.* **2019**, *168*, 83–94. [CrossRef]
10. Krot, A.N.; Keil, K.; Scott, E.R.D.; Goodrich, C.A.; Weisberg, M.K. 1.1—Classification of Meteorites and Their Genetic Relationships. In *Treatise on Geochemistry*; Elsevier: Amsterdam, The Netherlands, 2014; pp. 1–63.

11. McCoy, T.J.; Beck, A.W.; Prettyman, T.H.; Mittlefehldt, D.W. Asteroid (4) Vesta II: Exploring a geologically and geochem-ically complex world with the Dawn Mission. *Chem. der Erde-Geochem.* **2015**, *75*, 273–285. [CrossRef]
12. Cartwright, J.; Ott, U.; Mittlefehldt, D.; Herrin, J.; Herrmann, S.; Mertzman, S.; Mertzman, K.; Peng, Z.; Quinn, J. The quest for regolithic howardites. Part 1: Two trends uncovered using noble gases. *Geochim. Cosmochim. Acta* **2013**, *105*, 395–421. [CrossRef]
13. Cartwright, J.; Ott, U.; Mittlefehldt, D. The quest for regolithic howardites. Part 2: Surface origins highlighted by noble gases. *Geochim. Cosmochim. Acta* **2014**, *140*, 488–508. [CrossRef]
14. Eugster, O. Cosmic-ray Exposure Ages of Meteorites and Lunar Rocks and Their Significance. *Chem. der Erde-Geochem.* **2003**, *63*, 3–30. [CrossRef]
15. Eugster, O.; Herzog, G.; Marti, K.; Caffee, M. Irradiation records, cosmic-ray exposure ages, and transfer times of meteorites. In *Meteorites and The Early Solar System II*; University of Arizona Press: Tucson, AZ, USA, 2006; pp. 829–851.
16. Wieler, R. Cosmic-ray-produced noble gases in meteorites: Noble gases in geochemistry and cosmochemistry. *Rev. Mineral. Geochem.* **2002**, *47*, 125–170. [CrossRef]
17. Herzog, G.; Caffee, M.W. Cosmic-Ray Exposure Ages of Meteorites. In *Treatise on Geochemistry*; Elsevier: Amsterdam, The Netherlands, 2014; pp. 419–454. [CrossRef]
18. Welten, K.C.; Lindner, L.; Borg, K.; Loeken, T.; Scherer, P.; Schultz, L. Cosmic-ray exposure ages of diogenites and the recent collisional history of the howardite, eucrite and diogenite parent body/bodies. *Meteorit. Planet. Sci.* **1997**, *32*, 891–902. [CrossRef]
19. Farley, K.A. (U-Th)/He Dating: Techniques, Calibrations, and Applications. *Rev. Miner. Geochem.* **2002**, *47*, 819–844. [CrossRef]
20. Kelley, S. K-Ar and Ar-Ar dating. *Rev. Miner. Geochem.* **2002**, *47*, 785–818. [CrossRef]
21. Bogard, D.D. K–Ar ages of meteorites: Clues to parent-body thermal histories. *Chem. der Erde-Geochem.* **2011**, *71*, 207–226. [CrossRef]
22. Marchi, S.; Bottke, W.; Cohen, B.; de Sanctis, M.; Wuennemann, K.; McSween, H.; O'Brien, D.; Schenk, P.; Raymond, C.; Russell., C. A New Interpretation of ^{40}Ar-^{39}Ar Ages of Eucrites and Implications for Vesta's Collisional History. In Proceedings of the Lunar and Planetary Science Conference, Woodlands, TX, USA, 9–23 March 2012.
23. Chen, H.; Miao, B.; Huang, L. Ancient Silicification on Asteroid 4 Vesta: Evidence from a Eucrite Grove Mountains (GRV) 13001 from Antarctic. *LPI Contributions* **2015**, *1856*, 5003.
24. Ruzicka, A.; Grossman, J.; Bouvier, A.; Agee, C.B. The Meteoritical Bulletin, No. 103. *Meteorit. Planet. Sci.* **2017**, *52*, 1014. [CrossRef]
25. He, H.; Zhu, R.; Saxton, J. Noble gas isotopes in corundum and peridotite xenoliths from the eastern North China Craton: Implication for comprehensive refertilization of lithospheric mantle. *Phys. Earth Planet. Inter.* **2011**, *189*, 185–191. [CrossRef]
26. Su, F.; Xiao, Y.; He, H.; Su, B.; Wang, Y.; Zhu, R. He and Ar isotope geochemistry of pyroxene megacrysts and mantle xen-oliths in Cenozoic basalt from the Changle-Linqu area in western Shandong. *Chin. Sci. Bull.* **2014**, *59*, 396–411. [CrossRef]
27. Ranjith, P.; He, H.; Miao, B.; Su, F.; Zhang, C.; Xia, Z.; Xie, L.; Zhu, R. Petrographic shock indicators and noble gas signatures in a H and an L chondrite from Antarctica. *Planet. Space Sci.* **2017**, *146*, 20–29. [CrossRef]
28. Wang, Y.; He, H.; Zhang, C.; Su, F.; Padinhareveetil Manchan, R.; Ma, Y.; Zheng, D. Method of determining noble gases in trace meteorite specimens using a laser microprobe. *Acta Petrol. Sin.* **2018**, *34*, 3455–3466.
29. Wang, Y.; He, H.; Leya, I.; Ranjith, P.; Su, F.; Stephenson, P.; Zhang, C.; Zheng, D. The noble gases in five ordinary chondrites from Grove Mountains in Antarctica. *Planet. Space Sci.* **2020**, *192*, 105045. [CrossRef]
30. Ozima, M.; Podosek, F.A. *Noble Gas Geochemistry*; Cambridge University Press: Cambridge, UK, 2001. [CrossRef]
31. Matsuda, J.; Matsumoto, T.; Sumino, H.; Nagao, K.; Yamamoto, J.; Miura, Y.; Kaneoka, I.; Takahata, N.; Sano, Y. The 3He/4He ratio of the new internal He Standard of Japan (HESJ). *Geochem. J.* **2002**, *36*, 191–195. [CrossRef]
32. Eugster, O.; Lorenzetti, S.; Krähenbühl, U.; Marti, K. Comparison of cosmic-ray exposure ages and trapped noble gases in chondrule and matrix samples of ordinary, enstatite, and carbonaceous chondrites. *Meteor. Planet. Sci.* **2007**, *42*, 1351–1371. [CrossRef]
33. Swindle, T.D. Noble gases in the moon and meteorites: Radiogenic components and early volatile chronologies. *Rev. Miner. Geochem.* **2002**, *47*, 101–124. [CrossRef]
34. Ott, U. Noble Gases in Meteorites—Trapped Components. *Rev. Miner. Geochem.* **2002**, *47*, 71–100. [CrossRef]
35. Heber, V.S.; Wieler, R.; Baur, H.; Olinger, C.; Friedmann, T.A.; Burnett, D.S. Noble gas composition of the solar wind as collected by the Genesis mission. *Geochim. Cosmochim. Acta* **2009**, *73*, 7414–7432. [CrossRef]
36. Eugster, O.; Michel, T. Common asteroid break-up events of eucrites, diogenites, and howardites and cosmic-ray production rates for noble gases in achondrites. *Geochim. Cosmochim. Acta* **1995**, *59*, 177–199. [CrossRef]
37. Papike, J.J. Comparative Planetary Mineralogy: Chemistry of Melt-derived Pyroxene, Feldspar, and Olivine. In Proceedings of the Lunar and Planetary Science Conference, Houston, TX, USA, 16–20 March 1998.
38. Papike, J.J. *Planetary Materials: Reviews in Mineralogy*; Ribbe, P.H., Ed.; Mineralogical Society of America: Washington, DC, USA, 1998.
39. Papike, J.; Karner, J.M.; Shearer, C. Determination of planetary basalt parentage: A simple technique using the electron microprobe. *Am. Miner.* **2003**, *88*, 469–472. [CrossRef]
40. Merrill, R.B.; Ridings, R. *Basaltic Volcanism on the Terrestrial Planets*; Pergamon Press: New York, NY, USA, 1981; p. 1286.
41. Binnie, S.A.; Nishiizumi, K.; Welten, K.C.; Caffee, M.W.; Hoffmeister, D. Lunar surface processes inferred from cosmogenic radionuclides in Apollo 16 double drive core 68002/68001. *Geochim. Cosmochim. Acta* **2019**, *244*, 336–351. [CrossRef]

42. Wieler, R. Noble gases in the solar system. *Rev. Miner. Geochem.* **2002**, *47*, 21–70. [CrossRef]
43. Leya, I.; Neumann, S.; Wieler, R.; Michel, R. The production of cosmogenic nuclides by galactic cosmic-ray particles for 2π exposure geometries. *Meteorit. Planet. Sci.* **2001**, *36*, 1547–1561. [CrossRef]
44. Leya, I.; Masarik, J. Cosmogenic nuclides in stony meteorites revisited. *Meteorit. Planet. Sci.* **2009**, *44*, 1061–1086. [CrossRef]
45. Eugster, O.; Michel, T.; Niedermann, S.; Wang, D.; Yi, W. The record of cosmogenic, radiogenic, fissiogenic, and trapped noble gases in recently recovered Chinese and other chondrites. *Geochim. Cosmochim. Acta* **1993**, *57*, 1115–1142. [CrossRef]
46. Patzer, A.; Schultz, L.; Franke, L. New noble gas data of primitive and differentiated achondrites including Northwest Africa 011 and Tafassasset. *Meteorit. Planet. Sci.* **2003**, *38*, 1485–1497. [CrossRef]
47. Welten, K.C.; Nishiizumi, K.; Finkel, R.C.; Hillegonds, D.J.; Jull, A.J.T.; Franke, L.; Schultz, L. Exposure history and terrestrial ages of ordinary chondrites from the Dar al Gani region, Libya. *Meteorit. Planet. Sci.* **2004**, *39*, 481–498. [CrossRef]
48. Wieler, R.; Graf, T.; Signer, P.; Vogt, S.; Herzog, G.F.; Tuniz, C.; Fink, D.; Fifield, L.K.; Klein, J.; Middleton, R.; et al. Exposure history of the Torino meteorite. *Meteorit. Planet. Sci.* **1996**, *31*, 265–272. [CrossRef]
49. Scherer, P.; Herrmann, S.; Schultz, L. Noble gases in twenty-one Saharan LL-chondrites: Exposure ages and possible pairings. *Meteorit. Planet. Sci.* **1998**, *33*, 259–265. [CrossRef]
50. Welten, K.C.; Nishiizumi, K.; Caffee, M.W. Cosmogenic radionuclides in enstatite chondrites with low Ar-38/Ne-21 ex-posure age ratios. *Meteorit. Planet. Sci.* **2002**, *37*, A149.
51. Schmedemann, N.; Kneissl, T.; Ivanov, B.; Michael, G.; Wagner, R.J.; Neukum, G.; Ruesch, O.; Hiesinger, H.; Krohn, K.; Roatsch, T.; et al. The cratering record, chronology and surface ages of (4) Vesta in comparison to smaller asteroids and the ages of HED meteorites. *Planet. Space Sci.* **2014**, *103*, 104–130. [CrossRef]
52. Mandler, B.E.; Elkins-Tanton, L.T. The origin of eucrites, diogenites, and olivine diogenites: Magma ocean crystallization and shallow magma chamber processes on Vesta. *Meteorit. Planet. Sci.* **2013**, *48*, 2333–2349. [CrossRef]
53. Wang, D.; Lin, Y.; Liu, J. Cosmic-ray exposure and gas retention ages of the Guangmingshan (H5) chondrite. *Chin. Sci. Bull.* **2001**, *46*, 1544–1546. [CrossRef]